Wing and Conical Body of Arbitrary Cross Section in Supersonic Flow

Dan Mateescu*
McGill University, Montreal, Quebec, Canada

This paper presents an analysis of the combinations of wings and conical bodies of arbitrary cross section in supersonic flow. Particular emphasis is given to the delta wing and elliptic cone combinations, for which analytical solutions are obtained for the spanwise variation of the lifting load coefficient. Cases of subsonic and supersonic leading edges are both equally treated. In this formulation, the wing incidence is allowed to change along the span, as in the case of wing/body systems with leading-edge flaps, or with a continuously variable wing incidence. The effect of the wing thickness is also discussed. The theoretical solutions obtained for the delta wing and elliptic cone systems are in good agreement with Jorgensen's experimental results for various Mach numbers, wing spans, and cross-sectional semiaxis ratios. Good agreement with the experimental results is also obtained in the limit case of isolated elliptic cones.

Nomenclature

a,b = dimensionless semiaxes of the conical body cross section (Fig. 1)
b^* = vertical semiaxis in the complex plane x (Fig. 2), $=b/(1-B^2b^2)^{1/2}$
B = supersonic Prandtl-Glauert number, $=(M_\infty^2-1)^{1/2}$
$\mathfrak{B}$ = parameter of the Mach cone trace in the auxiliary complex plane X, defined by Eq. (27c)
c $=(a+b^*)/2$
C $=(\alpha-\alpha_0)U_\infty(1-B^2s^2)^{-1/2}$
C_L = lift coefficient based on the body cross-sectional area (as in Ref. 18)
$C_{L\alpha}$ = lift coefficient derivative with respect to the incidence α (or lift coefficient slope), $=dC_L/d\alpha$
C_p = pressure coefficient
C_t $=\gamma U_\infty(1-B^2a^2)^{-1/2}$
$F(x)$ = complex potential
$g(Y)$ = function resulting from the conformal transformation for elliptic cross sections, see Eq. (26)
$G_1(X,1/\mathfrak{B},L)$
$G_2(X,1/\mathfrak{B},L)$
$G(X,1/\mathfrak{B},L)$ = basic contributions of supersonic leading edges in the auxiliary complex plane X, defined by Eqs. (42) and (45)
$H_1(X,L,S)$
$H_2(X,L,S)$
$H(X,L,S)$ = basic contributions of subsonic ridges in the auxiliary complex plane X, defined by Eqs. (30) and (35)
k = cross-sectional semiaxis ratio of the conical body, $=b/a$
k^* = ellipticity ratio in the complex plane x, $=b^*/a$
K $=(\alpha-\alpha_0)U_\infty(1-B^2a^2)^{-1/2}$
ℓ = wing semispan (nondimensional, Fig. 1)
L = wing semispan in the auxiliary plane X, defined by Eq. (27a)
M_∞ = freestream Mach number
q $=\frac{1}{2}(a^2-b^{*2})^{1/2}$
Q $=\alpha U_\infty(B^2\ell^2-1)^{-1/2}$
Q_t $=\gamma U_\infty(1-B^2\ell^2)^{-1/2}$
s = hinge position of the leading-edge flaps (Fig. 1)
S = flap hinge position in the auxiliary plane X, defined by Eq. (27b)
u,v,w = perturbation velocity components due to the wing and body incidences
u_b,v_b,w_b = perturbation velocity components in the flow past the isolated conical body at zero angle of attack
$U(x),V(x),W(x)$ = complex functions associated with the perturbation velocity components u,v,w as in Eq. (4)
$U_F(X),V_F(X)$ = complex functions associated with the fictitious wing of variable incidence, and defined by Eqs. (17) and (20)
U_∞ = freestream velocity
x_1,x_2,x_3 = Cartesian coordinates
x = complex variable defined by Eqs. (3), $=y^*+iz^*$
X = auxiliary complex plane defined by the transformation of Eq. (12) or (23), $=Y+iZ$
y = nondimensional coordinate, $=x_2/x_1$
z = nondimensional coordinate, $=x_3/x_1$
α_0 = angle of attack of the body axis
α = wing incidence
$\pm\gamma$ = symmetrical thickness slope of the upper and lower wing surfaces
$\Delta C_p(y)$ = spanwise variation of the lifting load coefficient (dimensionless pressure between the lower and upper surfaces)

Presented as Paper 86-1826 at the AIAA 4th Applied Aerodynamics Conference, San Diego, CA, June 9-11, 1986; received Aug. 19, 1986; revision received Nov. 25, 1986.

*Associate Professor, Department of Mechanical Engineering (also Professor, Aeronautical Program, Ecole Polytechnique and Concordia University, Montreal, Canada) Member AIAA.

ϵ = an extremely small quantity, positively defined
χ, ζ = auxiliary complex planes

I. Introduction

THE analytical methods of solution present, in general, very good computing efficiency and possibly better accuracy in comparison with the computational methods, but they are usually subject to such limitations as: simpler geometrical configurations; same incidence of the wing and body, which implies constant wing incidence along the span; restrictions related to the flight regime that correspond to only subsonic or only supersonic leading edges; and additional restrictions such as the slender geometrical configuration assumption or the imposition of a minimum ratio of the wing span vs the transverse dimensions of the body.

For this reason, the computational methods are overwhelmingly preferred for the aerodynamic studies of complex aircraft configurations. In this situation, in addition to the academic interest, the role of the analytical methods remains to serve as a validation criterion for the computational methods (when no additional restrictive assumptions are made in deriving the analytical solutions) and to provide in some cases a more direct and physical insight related to the influence of the geometrical parameters on the local flow conditions, pressure distribution, and overall aerodynamic forces.

The steady supersonic conical potential flows have been investigated using various analytical methods of solution, a review of which can be found in Refs. 1–6, and more recently computational solutions have been obtained for these flows using conservative or nonconservative methods of approach.[7-8] The supersonic and hypersonic flows past a conical body alone with an elliptic or nearly circular cross section have been investigated analytically in Refs. 9–13, the constant-density approach being successfully used in the last references.

Analytical solutions of the attached supersonic flow past wing/body systems have been obtained using the assumption of slender geometrical configurations[14-16] or for systems with rectangular wings.[17] A very thorough experimental study has been conducted by Jorgensen[18] for isolated elliptic cones and for delta wing and elliptic cone combinations in supersonic flow.

A linear theory, without resorting to the additional restriction of the slender geometrical configuration, has been developed in Refs. 19–22 for the attached supersonic flow past wing (or cruciform wing) and circular conical body combinations. This theory has been extended to the case of an elliptic cone fitted with a delta wing having subsonic leading edges of the same incidence.[23]

The aim of the present work is to extend this method of solution to systems formed by a wing and a conical body of arbitrary cross section, with many of the above-mentioned restrictions eliminated. In this analysis, the wing incidence is considered, in general, different with respect to the angle of attack of the body axis and may change along the span. The case of wing/body systems with leading-edge flaps, or with a continuously variable wing incidence, can also be studied with this method of approach. The effect of the wing thickness on the perturbation velocities around the wing/body system can be determined using the same method of solution.

No restrictions are made regarding the supersonic flow regime in relation to the leading-edge sweep angles, the present method being able to handle both subsonic and supersonic leading edges. Also, no additional restrictions are made for the ratio of the wing and body spans; for this reason, the limit cases of the wing alone or the isolated conical body of arbitrary cross section can be obtained by simple particularization from the general wing/body solution, for vanishing vertical body axis ($b \to 0$) or when the wing span approaches the body span ($\ell = a$).

The present method of approach applies equally to the case of nonsymmetrical leading edges (with respect to the body axis) and can be eventually extended to the case of trapezoidal or polygonal wings fitted with conical bodies of arbitrary cross section. However, for the sake of simplifying the presentation, this analysis is restricted to the case of wing/body systems with symmetrical leading edges.

II. Perturbation Velocity Approach for Conical Flows

The wing and conical body system under consideration is represented in Fig. 1, in which the body cross section presents a double symmetry.

For an irrotational supersonic flow, the linear governing equation can be expressed in the form

$$-B^2\frac{\partial^2 q_k}{\partial x_1^2}+\frac{\partial^2 q_k}{\partial x_2^2}+\frac{\partial^2 q_k}{\partial x_3^2}=0 \qquad (k=1,2,3) \tag{1}$$

where $q_1=u$, $q_2=v$, and $q_3=w$ are the perturbation velocity components. In a conical flow, the perturbation velocity components are functions only of the dimensionless coordinates y and z,

$$y=x_2/x_1, \quad z=x_3/x_1 \tag{2}$$

such that Eq. (1) reduces to the two-dimensional form

$$(1-B^2y^2)\frac{\partial^2 q_k}{\partial y^2}+(1-B^2z^2)\frac{\partial^2 q_k}{\partial z^2}-2B^2yz\frac{\partial^2 q_k}{\partial y\partial z}$$

$$-2B^2y\frac{\partial q_k}{\partial y}-2B^2z\frac{\partial q_k}{\partial z}=0$$

the governing equation reduces further to the Laplace equation, $\nabla^{*2}q_k=0$, in an auxiliary plane defined by the geometrical transformation[2,19]

$$y^*=y/(1-B^2z^2), \quad z^*=[z/(1-B^2z^2)][1-B^2(y^2+z^2)]^{1/2} \tag{3}$$

The perturbation velocity components, which are harmonic functions in the complex plane $x=y^*+iz^*$, can be expressed as the real part of the associated complex functions

$$u(y^*,z^*)=\text{REAL } U(x), \quad v(y^*,z^*)=\text{REAL } V(x)$$

$$w(y^*,z^*)=\text{REAL } W(x) \tag{4}$$

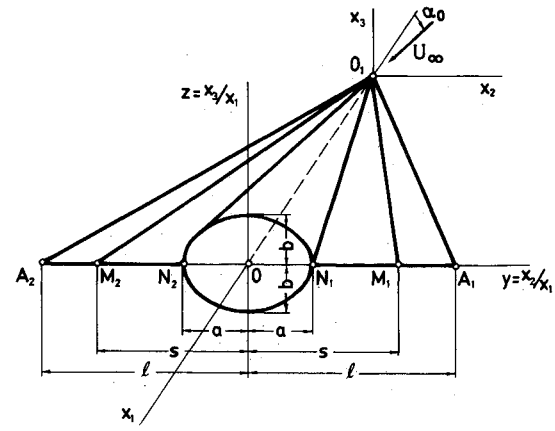

Fig. 1 Geometrical configuration of the wing/body system.

which are related by the compatibility relations

$$dU = -x\,dV = ix(1-B^2x^2)^{-1/2}\,dW \tag{5}$$

derived from the flow irrotationality conditions.[2]

In the auxiliary complex plane x, the wing trace remains unchanged ($z^*=0$, $y^*=y$), while the body cross section is swollen in the z direction, its vertical semiaxis becoming

$$b^* = b/(1-B^2b^2)^{1/2}$$

or

$$k^* = k/(1-k^2B^2a^2)^{1/2}, \quad (k=b/a, \quad k^*=b^*/a) \tag{6}$$

and the Mach cone trace in the physical plane $0yz$ is represented by the semiaxes $(-\infty, -1/B)$ and $(1/B, \infty)$, as shown in Fig. 2.

In the present approach, the supersonic flow past the isolated conical body at zero angle of attack, studied in Refs. 9–13, 24, and 25, is considered to be subtracted from the actual supersonic flow around the thin wing/body system. The resulting motion represents the effect of the wing and body incidences, determining the lifting load acting on the system, and it constitutes the object of the present analysis; in this motion, the perturbation velocity components u and v are antisymmetrically distributed with respect to the wing plane.

III. Method of Solution

To illustrate the method of solution, the wing incidence is assumed to be the same as the angle of attack α_0 of the body axis on the central wing portions N_1M_1 and N_2M_2 (Fig. 2), while having a different value α on the lateral portions M_1A_1 and M_2A_2, which can play the role of leading-edge flaps. The lines 0_1M_1 and 0_1M_2 (Fig. 1) across which the wing incidence suddenly changes are subsequently called "ridges."

Consider the complex potential $F(x)$ of the antisymmetrical motion in the auxiliary complex plane x, defined by its complex conjugate velocity in the form

$$\frac{dF}{dx} = V(x), \quad F(x) = U(x) + xV(x) \tag{7}$$

Assuming that the body vertex angle in the vertical plane is relatively small with respect to the Mach angle ($B^2b^2 \ll 1$) and using the compatibility relations [Eq. (5)], the complex conjugate velocity on the body becomes

$$\frac{dF}{dx} = V(x) = v - i(w + \alpha_0 U_\infty) \tag{8}$$

In the case of subsonic leading edges ($\ell < 1/B$), the boundary conditions for the antisymmetrical motion are expressed on the upper side of the wing and body in the complex form (using the compatibility relations)

$$\text{IMAG}\,[V(x)\,dx]_{\text{body}} = 0 \tag{9}$$

$$\text{IMAG}\,[V(x)]_{\text{wing}} = 0 \text{ for } |y^*| \in (a,s)$$

$$= C \text{ for } |y^*| \in (x,\ell) \tag{10}$$

where $C = (\alpha-\alpha_0)U_\infty(1-B^2s^2)^{-1/2}$ and outside the wing on the $0y^*$ axis

$$\text{REAL}\,U(y^*) = \text{REAL}\,V(y^*) = 0 \text{ for } |y^*| \in (\ell,\infty) \tag{11}$$

The constant C has been determined by integrating the compatibility relations of Eq. (5) around the ridge on a small semicircle of radius ϵ, nothing that $w(\ell+\epsilon) - w(\ell-\epsilon) = (\alpha_0-\alpha)U_\infty$.

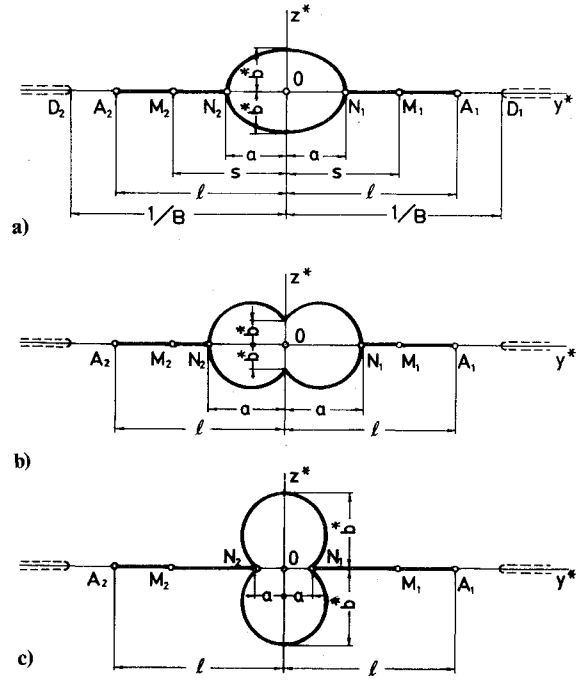

Fig. 2 Various cross-sectional shapes of the wing/body system represented in the complex plane $x = y^* + iz^*$.

The cross-sectional contour of the wing/body system can be mapped entirely onto the real axis in a complex plane $X = Y + iZ$ (Fig. 3) defined by convenient conformal transformations

$$\chi = f(x), \quad X = \chi + c^2/\chi \tag{12}$$

The actual function $f(x)$ depends on the shape of the body cross section, such as:

1) For an elliptic contour (Fig. 2a),

$$2\chi = x + (x^2 - 4q^2)^{1/2} \tag{13}$$

$$4q^2 = a^2 - b^{*2} = (1-k^{*2})a^2 \tag{14a}$$

$$2c = a + b^* = (1+k^*)a \tag{14b}$$

2) For a twin-circle contour (Fig. 2b),

$$\frac{x-hc}{x+hc} = \left(\frac{\chi-c}{\chi+c}\right)^h, \quad c = \frac{a}{h}, \quad h = \frac{4}{\pi}\cot^{-1}\frac{b^*}{a} \tag{15}$$

3) For a twin-circle contour with the centers on the vertical axis (Fig. 2c),

$$\frac{x-ihc}{x+ihc} = \left(\frac{\chi-ic}{\chi+ic}\right)^h, \quad c = \frac{b^*}{h}, \quad h = \frac{4}{\pi}\cot^{-1}\frac{a}{b^*} \tag{16}$$

Denoting the complex conjugate velocity in the X plane by

$$V_F(X) = \frac{dF}{dX} = V(x)\left(\frac{dx}{dX}\right) \tag{17}$$

the boundary conditions become

$$\text{IMAG } V_F(Y)=0 \quad \text{for } |Y|\in(-S,S) \tag{18}$$

$$=C\left(\frac{dx}{dX}\right)_{X=Y} \quad \text{for } |Y|\in(S,L)$$

$$\text{REAL } V_F(Y)=0 \quad \text{for } |Y|\in(L,\infty) \tag{19}$$

These boundary conditions correspond to those of a wing whose incidence is constant on its central portion M_2M_1 and variable on its lateral portions A_2M_2 and M_1A_1, for which the complex potential can be expressed, similar to Eq. (7), as

$$F(X)=U_F(X)+XV_F(X), \qquad dU_F=-X\,dV_F \tag{20}$$

Combining Eqs. (7) and (20), the complex function U on the wing/body system is expressed in terms of the corresponding solution of the variable incidence wing as

$$U=\left[U_F(X)+\left(X-x\frac{dX}{dx}\right)V_F(X)\right]_{x=y} \tag{21}$$

The spanwise variation of the lifting load coefficient $\Delta C_p(y)$ on the wing/body system can now be obtained from U, using the relation (see Appendix),

$$\Delta C_p=\text{REAL}[4U(y)/U_\infty] \tag{22}$$

A particular interest will be given in the following applications to the wing and elliptic cone combinations, for which

$$x=\frac{X+k^*(X^2-4c^2)^{1/2}}{1+k^*} \tag{23}$$

$$\left(\frac{dx}{dX}\right)_{X=Y}=\frac{1+k^*Y(Y^2-4c^2)^{-1/2}}{1+k^*} \tag{24}$$

$$\left[X-x\left(\frac{dX}{dx}\right)\right]_{X=Y}=(1+k^*)g(Y) \tag{25}$$

$$g(Y)=\frac{k^*}{1+k^*}\,\frac{4c^2}{k^*Y+(Y^2-4c^2)^{1/2}} \tag{26}$$

$$L=\frac{\ell-k^*(\ell^2-4q^2)^{1/2}}{1-k^*} \tag{27a}$$

$$S=\frac{s-k^*(s^2-4q^2)^{1/2}}{1-k^*} \tag{27b}$$

$$1/\mathfrak{B}=\frac{1/B-k^*(1/B^2-4q^2)^{1/2}}{1-k^*} \tag{27c}$$

IV. Wing and Elliptic Cone Systems with Subsonic Leading Edges

The solution for the fictitious wing of variable incidence, defined by the boundary conditions [Eqs. (18) and (19)], is determined using the method of perturbation velocity singularities, as developed in Refs. 2, 20, and 22. In the present analysis, the flow is assumed attached at the subsonic leading edges, although this method of approach can eventually be extended to take into consideration the main effects of the leading-edge flow separation. As indicated by the experimental results for isolated wings, the pressure distribution in the vicinity of a subsonic leading edge is strongly affected by the flow separation. For high angles of attack and slender wings ($B\ell$ much smaller than unity), the flow separation has an important overall effect on the lift coefficient C_L. In these cases, the leading-edge flow separation introduces a nonlinear dependence of the lift coefficient on the incidence $C_L(\alpha)$. However, the overall effects of the flow separation are less important for small angles of attack and not so slender geometrical configurations in the supersonic regime, characterized by a wing vertex angle not so small with respect to the Mach angle (i.e., when $B\ell$ is not much smaller than unity; in fact, this type of flow separation does not occur at all when the leading edges become supersonic $B\ell>1$). In these cases, the lift coefficient depends linearly (or almost) on the wing incidence, a fact that is confirmed by the experimental results obtained for the wing and body combinations, which are discussed further in Sec. VIII.

The analysis of the attached flow in the vicinity of the leading edges[2] has shown that the perturbation velocity components (in particular, u and v) present the singularities $(\ell\pm y)^{-1/2}$. In the complex form $(L\pm X)^{-1/2}$, these leading-edge singularities also have to be present in the functions $U_F(X)$ and $V_F(X)$, which are associated with the perturbation velocity components of the variable incidence fictitious wing defined in Sec. III.

Both the actual and fictitious wings present sudden changes of incidence along the ridges 0_1M_1 and 0_1M_2 ($y=\pm s$, $Y=\pm S$), which are associated, as shown in Ref. 2, with source-type velocity singularities $\ell n(y\pm s)$; these singularities become $\ell n(X\pm S)$ for the functions U_F and V_F.

The following complete expressions of the leading-edge and ridge singularities, satisfying the set of corresponding boundary conditions on the wing and outside it, are used in the expression of the complex function $V_F(X)$:

$$A_0\left(\frac{L+X}{L-X}\right)^{1/2}, \quad -A_0\left(\frac{L-X}{L+X}\right)^{1/2} \tag{28}$$

$$\Delta[\text{IMAG}V_F(Y)]_{Y=S}H_1(X,L,S) \tag{29a}$$

$$-\Delta[\text{IMAG}V_F(Y)]_{Y=-S}H_2(X,L,S) \tag{29b}$$

where $\Delta[\text{IMAG}V_F(Y)]_{Y=\pm S}$ represent the sudden changes in the imaginary part of $V_F(Y)$ at the ridges and where

$$H_1(X,L,S)=\frac{2}{\pi}\cosh^{-1}\sqrt{\frac{(L-X)(L+S)}{2L(S-X)}} \tag{30a}$$

$$H_2(X,L,S)=\frac{2}{\pi}\cosh^{-1}\sqrt{\frac{(L+X)(L+S)}{2L(S+X)}} \tag{30b}$$

These expressions were determined in another auxiliary plane,[2] $\zeta=[(L-X)/(L+X)]^{1/2}$, by combining the leading-edge and ridge singularities $1/\zeta$, ζ and $\ell n(\zeta\pm\sigma)$, $\ell n(\zeta\pm 1/\sigma)$, where $\sigma=[(L-S)/(L+S)]^{1/2}$, in order to satisfy the corresponding set of boundary conditions.

In addition to the above contributions of the leading edges and ridges, a continuous distribution of elementary ridges is used to represent the fictitious wing portions with variable incidence defined by the boundary condition [Eq. (18)]. In this manner, the solution for the function V_F is

$$V_F(X)=-AX(L^2-X^2)^{1/2}$$

$$+C\left(\frac{dx}{dX}\right)_{X=Y}\left[H_1(X,L,S)-H_2(X,L,S)\right]$$

$$+C\int_S^L\left[H_1(X,L,T)-H_2(X,L,T)\right]\left(\frac{dx}{dX}\right)_{X=Y}dT \tag{31}$$

A similar expression is established for $U_F(X)$, using the compatibility relation $dU_F = -X dV_F$ for the fictitious wing. The axial perturbation velocity u and the spanwise variation of the lifting load coefficient ΔC_p on the wing/body system are then determined from Eqs. (21) and (22).

The following solutions are obtained for various wing and elliptic cone combinations, using Eqs. (23-27) to define the fictitious wing solution in the X plane.

Delta Wing and Elliptic Cone System

When the entire wing has the incidence α different from the angle of attack α_0 of the body axis (i.e., when $s=a$ and $S=2c$), the spanwise variation of the lifting load coefficient ΔC_p is determined by inserting the following solution in Eq. (22):

$$U(Y) = A[L^2 - (1+k^*)Yg(Y)](L^2 - Y^2)^{-1/2} - K[a-g(Y)]H_1(Y,L,2c) - K[a+g(Y)]H_2(Y,L,2c) - iKg(Y) \quad (32)$$

where $K = (\alpha - \alpha_0)U_\infty(1-B^2a^2)^{-1/2}$ and the constant A is determined from the condition[2]

$$\text{IMAG}\int_{\ell-\epsilon}^{1/B} \frac{(1-B^2x^2)^{1/2}}{x} dU = w\left(\frac{1}{B}\right) - w(\ell-\epsilon) = \alpha U_\infty \quad (33)$$

The influence of the ellipticity parameter $k=b/a$ (the ratio of the ellipse semiaxes) on the spanwise variation of the lifting load coefficient ΔC_p is shown in Fig. 4 for the case when the wing has the same incidence as the body axis ($\alpha=\alpha_0$, with $B\ell=0.8$). As shown in Fig. 4, the particular cases of the wing alone ($k=b/a=0$) and the isolated cruciform wing ($k\to\infty$) are obtained without difficulties from the general solution [Eq. (32)], since no restrictions have been imposed on the ellipticity ratio k.

Wing/Body System with Leading-Edge Flaps

Consider the case defined by the boundary conditions [Eq. (18)], when the wing has the same incidence α_0 as the body axis on its central portions ($a<|y|<s$) and a different incidence α on the lateral portions ($s<|y|<\ell$), which can play the role of leading-edge flaps. In this case, the solution is

$$U(Y) = A[L^2 - (1+k^*)Yg(Y)](L^2 - Y^2)^{-1/2} - C[s-g(Y)]H_1(Y,L,S) - C[s+g(Y)]H_2(Y,L,S) - Cg(Y)H(Y,L,S) \quad (34)$$

where $C = (\alpha-\alpha_0)U_\infty(1-B^2s^2)^{-1/2}$, A is determined using the same condition as Eq. (33), and

$$H(Y,L,S) = \frac{2}{\pi}\cosh^{-1}\sqrt{\frac{(L^2-Y^2)(S^2-4c^2)}{(L^2-4c^2)(S^2-Y^2)}} \quad (35)$$

Limit Case of the Isolated Elliptic Cone

The limit cases of the isolated wing ($b=0$) and of the isolated elliptic cone ($\ell=a$) can be obtained from Eq. (32) particularized for $\alpha=\alpha_0$ (i.e., $K=0$), since no restrictions whatsoever have been introduced during the derivation process regarding the ratios of the body semiaxes vs the wing span.

For an isolated elliptic cone at the angle of attack α, the spanwise distribution of the lifting load coefficient is

$$\Delta C_p = 4\alpha a^2 A_1 \frac{[(1+k^*)^2a^2 - Y^2]^{1/2}}{(1+k^*)^2a^2 - (1-k^{*2})Y^2} \quad (36)$$

In this case, the singularities $(4c^2-Y^2)^{-1/2}$, introduced by the transformation of Eqs. (23) and (24) in $U_F(X)$ and $V_F(X)$ at the fictitious wing leading edges ($Y=\pm 2c$), are canceled in the complex function $U(x)$ calculated with Eq. (21) on the wing/body system. The constant A_1 is determined from the following condition, obtained by integrating the compatibility relations [Eq. (5)] along the imaginary axis ($x=iz^*$):

$$\text{REAL}\int_{b^*}^{\infty} \frac{(1+B^2z^{*2})^{1/2}}{z^*} d[U(iz^*)] = -\alpha U_\infty + \text{REAL}[bU(ib^*)] \quad (37)$$

where $U(x)$ represents the solution of the complex function associated to the axial perturbation velocity, in this case,

$$U(x) = i\alpha U_\infty a^2 [A_1/(1+k^*)][x^2 - (1-k^{*2})a^2]^{-1/2} \quad (38)$$

V. Wing and Elliptic Cone Systems with Supersonic Leading Edges

When the leading edges of the wing are supersonic ($\ell > 1/B$), the second part of the boundary condition [Eq. (10)] is replaced by

$$\text{IMAG } V(y^*) = C \quad \text{for } |y^*| \in (s, 1/B) \quad (39a)$$

$$\text{REAL } V(y^*) = -Q \quad \text{for } |y^*| \in (1/B, \ell) \quad (39b)$$

where $Q = \alpha U_\infty (B^2\ell^2 - 1)^{-1/2}$; this value of Q is determined by integrating the compatibility relations [Eq. (5)] around the leading edges, along a semicircle of a small radius ϵ, noting that $w(\ell+\epsilon) - w(\ell-\epsilon) = \alpha U_\infty$. The second part of the boundary condition of Eq. (18), where $L > /\mathfrak{B}$ in this case, is replaced accordingly by

$$\text{IMAG } V_F(Y) = C\left(\frac{dx}{dX}\right)_{X=Y} \quad \text{for } |Y| \in (S, 1/\mathfrak{B})$$

$$\text{REAL } V_F(Y) = -Q\left(\frac{dx}{dX}\right)_{X=Y} \quad \text{for } |Y| \in (1/\mathfrak{B}, L) \quad (40)$$

The perturbation velocity components are suddenly changing their values across the leading edges, which are in this case associated to vortex-type singularities[2] $i\ell_n(x \pm \ell)$ in the expressions of the complex functions $U(x)$ and $V(x)$. The complete expressions of the leading-edge singularities satisfying the corresponding set of boundary conditions of the complex function $V_F(X)$ are

$$\Delta[\text{REAL } V_F(Y)]_{Y=L} \quad G_1(X, 1/\mathfrak{B}, L)$$
$$-\Delta[\text{REAL } V_F(Y)]_{Y=-L} \quad G_2(X, 1/\mathfrak{B}, L) \quad (41)$$

where $\Delta[\text{REAL } V_F(Y)]_{Y=\pm L}$ represent the sudden changes in the real part of $V_F(Y)$ at the leading edges, and where

$$G_1(X, 1/\mathfrak{B}, L) = \frac{2}{\pi}\cos^{-1}\sqrt{\frac{(1/\mathfrak{B}-X)(1/\mathfrak{B}+L)}{2/\mathfrak{B}(L-X)}} \quad (42a)$$

$$G_2(x, 1/\mathfrak{B}, L) = \frac{2}{\pi}\cos^{-1}\sqrt{\frac{(1/\mathfrak{B}+X)(1/\mathfrak{B}+L)}{2/\mathfrak{B}(L+X)}} \quad (42b)$$

The solution for the fictitious wing in the X plane is then determined in the same way as in Sec. IV, that is

$$V_F(X) = -Q\left(\frac{dx}{dX}\right)_{X=L}\left[G_1\left(X,\frac{1}{\mathfrak{B}},L\right)+G_2\left(X,\frac{1}{\mathfrak{B}},L\right)\right]$$
$$+Q\int_{1/\mathfrak{B}}^{L}\left[G_1\left(X,\frac{1}{\mathfrak{B}},L\right)+G_2\left(X,\frac{1}{\mathfrak{B}},L\right)\right]\left(\frac{dx}{dX}\right)_{X=T}dT$$
$$+C\left(\frac{dx}{dX}\right)_{X=S}\left[H_1\left(X,\frac{1}{\mathfrak{B}},S\right)-H_2\left(X,\frac{1}{\mathfrak{B}},S\right)\right]$$
$$+C\int_{S}^{1/\mathfrak{B}}\left[H_1\left(X,\frac{1}{\mathfrak{B}},T\right)-H_2\left(X,\frac{1}{\mathfrak{B}},T\right)\right]\left(\frac{dx}{dX}\right)_{X=T}dT \tag{43}$$

This equation is applied as follows for various wing and elliptic cone systems with supersonic leading edges.

Delta Wing and Elliptic Cone System

When the entire wing has an incidence α different from the angle of attack α_0 of the body axis (i.e., $s=a$, $S=2c$), the solution for the antisymmetrical motion around the wing/body system is

$$U(Y) = Q[\ell-g(Y)]G_1(Y,1/\mathfrak{B},L)$$
$$+Q[\ell+g(Y)]G_2(Y,1/\mathfrak{B},L)+Qg(Y)G(Y,1/\mathfrak{B},L)$$
$$-K[a-g(Y)]H_1(Y,1/\mathfrak{B},2c)$$
$$-K[a+g(Y)]H_2(Y,1/\mathfrak{B},2c)-iKg(Y) \tag{44}$$

where

$$G\left(Y,\frac{1}{\mathfrak{B}},L\right)=\frac{2}{\pi}\cos^{-1}\sqrt{\frac{(1/\mathfrak{B}^2-Y^2)(L^2-4c^2)}{(1/\mathfrak{B}^2-4c^2)(L^2-Y^2)}} \tag{45}$$

The typical spanwise variation of the lifting load coefficient ΔC_p, which is obtained from Eq. (22), is shown in Fig. 5 for the cases when the wing incidence α is the same as the angle of attack α_0 of the body axis, double ($\alpha=2\alpha_0$), or half of it ($\alpha=0.5\alpha_0$). The geometry of the delta wing and elliptic cone system considered in Fig. 5 is defined by $B\ell=1.5$, $Ba=0.5$, $k=b/a=0.5$.

Wing/Body System with Leading-Edge Flaps

Consider two leading-edge flaps A_2M_2 and M_1A_1 (Fig. 2a) having the incidence α, while the rest of the wing and the body axis are at the angle of attack α_0. The solution for $s<1/B$ (or $\mathfrak{B}S<1$) is in this case

$$U(Y) = Q[\ell-g(Y)]G_1(Y,1/\mathfrak{B},L)$$
$$+Q[\ell+g(Y)]G_2(Y,1/\mathfrak{B},L)+Qg(Y)G(Y,1/\mathfrak{B},L)$$
$$-C[s-g(Y)]H_1(Y,1/\mathfrak{B},S)$$
$$-C[s+g(Y)]H_2(Y,1/\mathfrak{B},S)-Cg(Y)H(Y,1/\mathfrak{B},S) \tag{46}$$

A similar expression can be obtained for $s>1/B$.

VI. Extension to the Case of Variable Wing Incidence

The present method of approach can be extended to solve the antisymmetrical motion past wing/body systems in the case when the wing incidence has a continuous conical variation along the span $\alpha(y)$. A continuous distribution of elementary ridges corresponding to the incidence variation has to be considered on the actual wing. In the case of subsonic leading edges ($\ell<1/B$), a pair of such elementary ridges situated at $y=\pm s$ are represented by an elementary contribution defined by Eq. (34), where C has to be replaced by

$$[d\alpha(y)]_{y=s}U_\infty(1-B^2s^2)^{-1/2}$$

The general solution is expressed in this case as

$$U(Y) = A[L^2-(1+k^*)Yg(Y)](L^2-Y^2)^{-1/2}$$
$$-U_\infty\int_a^\ell\left(\frac{d\alpha}{dy}\right)_{y=s}(1-B^2s^2)^{-1/2}[s-g(Y)]H_1(Y,L,S)$$
$$+[s+g(Y)]H_2(Y,L,S)+g(Y)H(Y,L,S)ds \tag{47}$$

The solution for the case of supersonic leading edges is obtained in a similar manner.

VII. Effect of the Wing Thickness

Consider that the wing has a symmetrical thickness defined by the slope $\pm\gamma$ on the upper and lower surfaces, respectively, while the wing and body incidences are assumed zero.

The motion considering the effect of the wing thickness is defined, when $\ell<1/B$, by the following boundary conditions on the upper surface of the system:

$$\text{IMAG}\,[V(x)dx]_{\text{body}}=0 \tag{48}$$

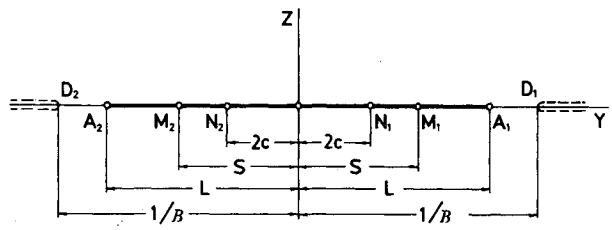

Fig. 3 Wing/body configuration in the auxiliary complex plane $X=Y+iZ$.

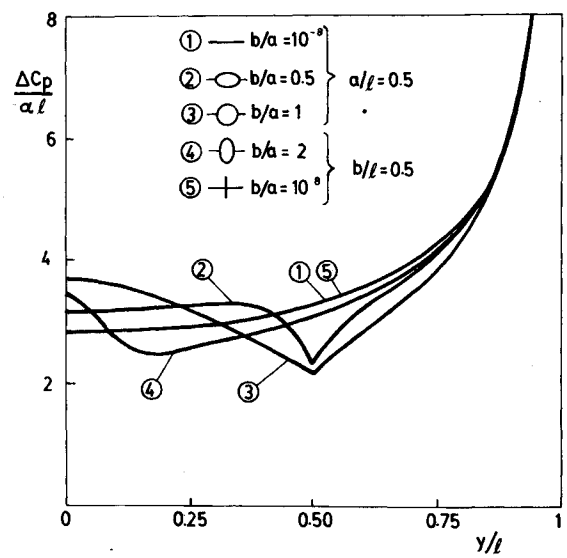

Fig. 4 Influence of the ellipse semiaxis ratio $k=b/a$ on the spanwise variation of the lifting load coefficient ΔC_p for a delta wing and elliptic cone system ($\alpha=\alpha_0$; $B\ell=0.8$).

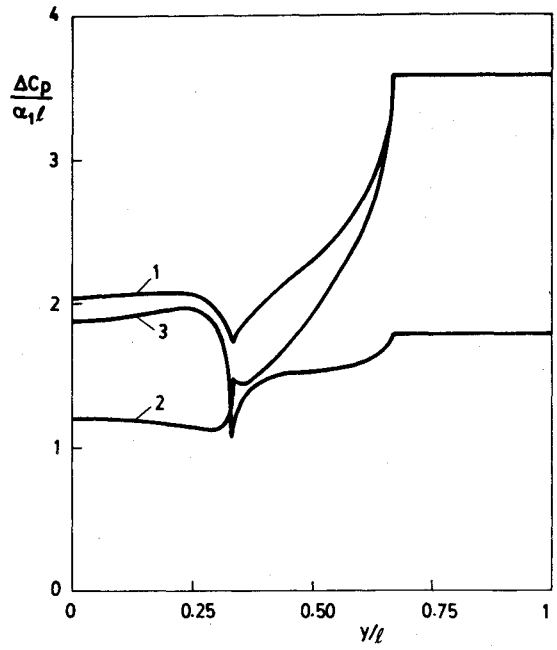

Fig. 5 Typical spanwise variation of the lifting load coefficient ΔC_p on the delta wing and elliptic cone system ($B\ell=1.5$, $Ba=0.5$, $k=b/a=0.5$). Curve 1: $\alpha=\alpha_1$ and $\alpha_0=\alpha_1$; curve 2: $\alpha=\alpha_1$ and $\alpha_0=0.5\ \alpha_1$; curve 3: $\alpha=0.5\ \alpha_1$ and $\alpha_0=\alpha_1$.

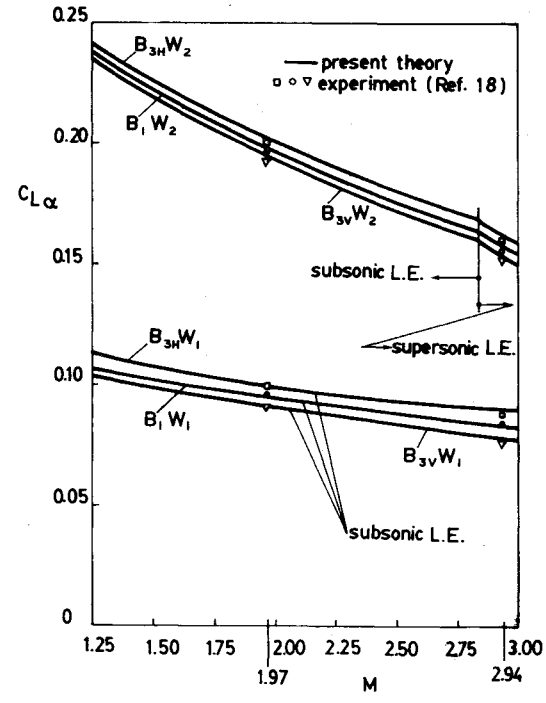

Fig. 6 Theoretical lift coefficient derivative $C_{L\alpha}=dC_L/d\alpha$ of delta wing and elliptic cone configurations vs Mach number compared with Jorgensen's experimental results.[18]

$$\text{IMAG}\,[V(x)]_{z=0} = -C_t \qquad \text{for } |y^*| \in (a,\ell)$$
$$= Q_t - C_t \qquad \text{for } |y^*| \in (\ell, 1/b) \tag{49}$$

$$\text{REAL}\,[V(x)]_{z=0} = \text{REAL}\,[U(x)]_{z=0} = 0$$
$$\text{for } |y^*| \in (1/B, \infty) \tag{50}$$

where $C_t=\gamma U_\infty (1-B^2a^2)^{-1/2}$ and $Q_t=\gamma U_\infty (1-B^2\ell^2)^{-1/2}$.

The axial perturbation velocity in this motion, $u=\text{REAL}\,[U(Y)]$, which is symmetric with respect to the wing plane, can be determined in the same manner as above,

$$\begin{aligned} U(Y) = &-Q_t[\ell - g(Y)]H_1(Y,1/\mathcal{B},L) \\ &-Q_t[\ell + g(Y)]H_2(Y,1/\mathcal{B},L) - Q_t g(Y) H(Y,1/\mathcal{B},L) \\ &+C_t[a - g(Y)]H_1(Y,1/\mathcal{B},2c) \\ &+C_t[a + g(Y)]H_2(Y,1/\mathcal{B},2c) + iC_t g(Y) \end{aligned} \tag{51}$$

A similar solution is obtained when $\ell > 1/B$.

The same method can also be extended to solve the case when the wing thickness slope has a continuous conical variation along the span, $\gamma(y)$.

VIII. Comparison with Experimental Results

To validate the present method of approach, the theoretical solutions obtained in the previous sections are compared with the available experimental results.

Such a comparison is given in Fig. 6 for the lift coefficient slope $C_{L\alpha}=dC_L/d\alpha$ of the delta wing and elliptic cone combinations tested by Jorgensen[18] at two different Mach numbers, $M_\infty=1.97$ and 2.94. The wing/body systems tested by Jorgensen represent the combinations of two different wings (W_1 and W_2) with the semispans $\ell=0.2507$ and 0.3760, respectively, and three elliptic cones (B_{3H}, B_1, and B_{3V}) and are geometrically defined as follows: $B_{3H}W_1-k=1/3$, $a/\ell=0.9413$; $B_1W_1-k=1$, $a/\ell=0.5435$; $B_{3V}W_1-k=3$, $a/\ell=0.3138$; $B_{3H}W_2-k=1/3$, $a/\ell=0.6276$; $B_1W_2-k=1$, $a/\ell=0.3623$; $B_{3V}W_2-k=3$, $a/\ell=0.2092$.

The comparison made in Fig. 6 shows a good agreement between the present theoretical results, derived in Secs. IV and V, and the experimental lift coefficient slope $C_{L\alpha}$ at small angles of attack. This good agreement is also maintained at higher incidences (α up to 12 deg or even higher) for the configurations $B_{3H}W_2$, B_1W_2, and $B_{3V}W_2$ at both Mach numbers 1.97 and 2.94, for which a remarkable linear variation of the lift coefficient with the angle of attack α can be observed in Figs. 8 and 9 of Ref. 18; to a somewhat lesser extent (α up to about 8 deg), the agreement also holds for the configurations $B_{3H}W_1$, B_1W_1, and $B_{3V}W_1$ at the Mach number $M_\infty=2.94$, for which the lift coefficient varies almost linearly with the incidence, as shown in Fig. 7 of Ref. 18. The lift coefficient of the later configurations at the Mach number 1.97 (for which $B\ell=0.4254$) is slightly nonlinear with respect to the incidence, as shown in Fig. 6 of Ref. 18; this indicates that the effect of the leading-edge flow separation should be considered for configurations having $B\ell<0.5$ or even at higher values of $B\ell$ for an accurate prediction of the lifting load coefficient in the vicinity of leading edges.

In Fig. 7, the theoretical solution derived in Sec. IV for the limit case of the isolated elliptic cone is compared with the experimental values of the lift coefficient slope at small angles of attack. The experimental results are obtained by Jorgensen[18] at Mach numbers 1.97 and 2.94 for the following elliptic cones: $B_{4H}-k=1/6$, $a=0.3337$; $B_{3H}-k=1/3$, $a=0.2360$; $B_{2H}-k=2/3$, $a=0.1669$; $B_{1H}-k=1$, $a=0.1362$; $B_{2V}-k=1.5$, $a=0.1112$; and $B_{3V}-k=3$, $a=0.0787$.

A good agreement can also be observed in the cases when the cone semivertex angle in the vertical plane is small with respect to the Mach angle ($Bb<0.4$). However, in these cases, the agreement is restricted mainly to small incidences, since the flow separation becomes particularly important for $Ba<0.4$; this fact is confirmed by the increased nonlinearity of the experimental lift coefficient shown in Figs. 3 and 4 of Ref. 18.

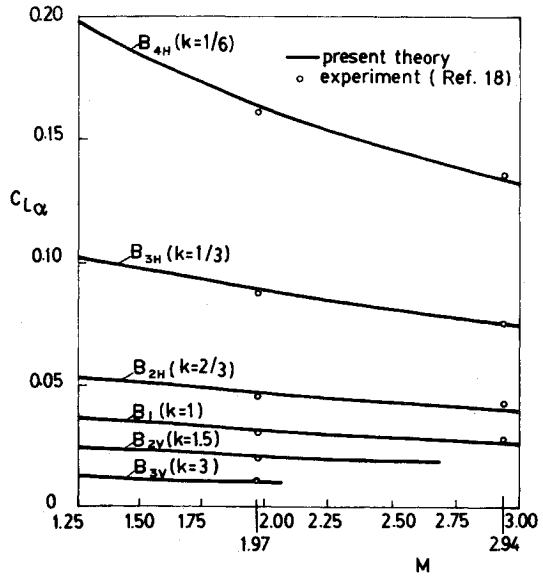

Fig. 7 Theoretical lift coefficient derivative $C_{L\alpha}$ of isolated elliptic cones vs Mach number, compared with Jorgensen's experimental results.[18]

In Figs. 6 and 7 the lift coefficient is based on the cross-sectional area of the elliptic cone, as in Ref. 18, and the incidences are considered in degrees.

IX. Conclusions

The objective of this paper was the analysis of the attached supersonic flow past a wing and conical body having arbitrary cross-section combinations.

In this analysis, the wing incidence (which is assumed to be different from the angle of attack of the body axis) is allowed to change along the span as in the cases of wing/body systems with leading-edge flaps or with a continuously variable wing incidence. Cases of both subsonic and supersonic leading edges are treated. The effect of the wing thickness on the perturbation velocities is also determined using the same method of approach.

Particular emphasis is given to the wing and elliptic cone combinations, for which analytical solutions are obtained for the spanwise variation of the lifting load coefficient.

The limit cases of the isolated wing (or cruciform wing) and the isolated elliptic cone are obtained from the general solution by simple particularization, since no additional restrictive assumptions were introduced in the derivation process.

The validity of the present method of solution is established by comparison with the experimental results obtained by Jorgensen[18] for delta wing and elliptic cone configurations and for isolated elliptic cones.

A good agreement was observed between the theoretical lift coefficient derivative, based on the solutions obtained in this analysis, and Jorgensen's experimental results. The agreement is good for all wing/body combinations and for the isolated elliptic cones tested by Jorgensen at two Mach numbers, 1.97 and 2.94, and characterized by various ellipse semiaxis ratios. For the systems with larger wing semiapex angle, the agreement is extended on a relatively large domain of incidences, for cases of both subsonic and supersonic leading edges. However, for the systems with a small wing semiapex angle compared to the Mach angle and for the slender isolated cones, the agreement is restricted to small incidences; this is due to the flow separation at the subsonic leading edges, which becomes particularly important for very slender configurations. The present approach is eventually susceptible to extension in order to consider the effect of the leading-edge flow separation.

Appendix

The lifting load coefficient has been calculated in the numerical examples given above by using Eq. (22), based on the linear relation of the pressure coefficient, which is consistent with the linear analysis developed in the present paper.

Alternatively, using the second-order relation of the pressure coefficient in the system of coordinates related to the body axis (see Fig. 1), the lifting load coefficient is expressed as

$$\Delta C_p = 4\left[\frac{u}{U_\infty} + \frac{v_b v + w_b(w+\alpha_0 U_\infty)}{U_\infty^2} - \frac{u_b u}{U_\infty^2}(M_\infty^2 - 1)\right] \quad \text{(A1)}$$

where u_b, v_b, w_b and u, v, w are the perturbation velocity components in the flow past the conical body at zero angle of attack and in the antisymmetrical motion (with respect to the $0y$ axis) due to the wing and body incidences, respectively. The last term is always negligible in comparison with the first one. The other double product terms, $v_b v/U_\infty^2$ and $w_b(w+\alpha_0 U_\infty)/U_\infty^2$, obviously become zero for $y=0$, $y=\pm a$, and $|y| \geq 1/B$, although they do not always have negligible values with respect to u/U_∞; this fact was first mentioned by Spreiter[15] for the double product $v_b v$ on thin wing in the case of slender wing/body combinations.

However, on the elliptic cone the double products $v_b v$ and $w_b(w+\alpha_0 U_\infty)$ have opposite signs and they cancel each other within the accepted accuracy of the present analysis; for this reason, Eqs. (22) and (A1) provide practically the same results for the lift coefficient of the elliptic cone.

With regard to the lift of the wing, the differences in the results obtained for a perfectly thin wing with the Eqs. (22) and (A1) can, in some cases, be larger than for the body, although they are smaller than those calculated with the slender-body theory and they tend to become zero when the ratio a/ℓ is small or is close to the unity; moreover, on the supersonic part of the wing ($|y| \geq 1/B$), $u_b = v_b = w_b = 0$ and hence the second-order relation [Eq. (A1)] reduces to the linear equation (22). However, Eq. (A1) does not take into account the effects of the wing thickness, which actually occur even in the case of a perfectly thin wing due to the boundary-layer thickness on the upper and lower surfaces. When the wing thickness effects are considered in the second-order relation of the lifting load coefficient, the differences in the overall lift tend to be, in all cases, of the same order of magnitude as the approximations already accepted in this linear analysis, which presently do take into account neither the nonlinear effects of the leading-edge flow separation nor those of the wing thickness. As mentioned above, Jorgensen's experimental results[18] show that the nonlinear effects of the flow separation at the leading edges become important when $B\ell < 0.5$ or, in the case of the isolated elliptic cone, when $Ba < 0.5$.

For this reason, the linear relation of the lifting load coefficient [Eq. (22)], which is entirely consistent with the present linear analysis, was used in calculating the numerical examples given above. The linear relation also presents the advantage of being simple to use and not dependent on the previous determination of the perturbation velocities in the flow past the conical body at zero angle of attack.

References

[1]Jones, R. T. and Cohen, D., *High Speed Wing Theory*, Princeton University Press, Princeton, NJ, 1960.

[2]Carafoli, E., Mateescu, D., and Nastase, A., *Wing Theory in Supersonic Flow*, Pergamon Press, New York, 1969, pp. 27-107.

[3]Fenain, M., "La théorie des écoulements á potential homogéne et ses applications au calcul des ailes en régime supersonique," *Progress in Aeronautical Sciences*, Vol. I, edited by Kuchemann, A. Ferri, and L. H. F. Sterne, Pergamon Press, New York, 1961, pp. 26-103.

[4]Kuckemann, D., "Aircraft Shapes and Their Aerodynamics for Flight at Supersonic Speeds," *Advances in Aeronautical Sciences*, Vol. 3, Pergamon Press, New York, 1961, pp. 221-275.

[5]Ward, G. N., *Linearized Theory of Steady High-Speed Flow*, Cambridge University Press, London 1955, pp. 135-164.

[6]Lawrence, H. R. and Flax, A. H., "Wing-Body Interference at Subsonic and Supersonic Speeds. Survey and New Developments," *Journal of the Aeronautical Sciences*, Vol. 21, 1954, pp. 289-324.

[7]Grossman, B., "Numerical Procedure for the Computation of Irrotational Conical Flows," *AIAA Journal*, Vol. 17, Aug. 1979, pp. 828-837.

[8]Bradley, P. F., Dwoyer, D. L., and South, J. C., "Vectorized Schemes for Conical Potential Flow Using the Artificial Density Method," *AIAA Journal*, Vol. 24, Jan. 1986, pp. 13-20.

[9]Ferri, A., Ness, N., and Kaplita, T. T., "Supersonic Flow over Conical Bodies without Axial Symmetry," *Journal of the Aeronautical Sciences*, Vol. 20, Aug. 1953, pp. 563-571.

[10]Fraenkel, L. E., "Supersonic Flow past Slender Bodies of Elliptic Cross Section," British Aeronautical Research Council, R&M 2954, 1955.

[11]Mascitti, V. R., "Calculation of Linearized Supersonic Flow over Slender Cones of Arbitrary Cross Section," NASA TN D-6818, July 1972.

[12]Lee, H. M. and Rasmussen, M. L., "Hypersonic Flow Past an Elliptic Cone," AIAA Paper 79-0364, Jan. 1979.

[13]Jischke, M., "Supersonic Flow Past Conical Bodies with Nearly Circular Cross-Sections," *AIAA Journal*, Vol. 19, Feb 1981, pp. 242-245.

[14]Spreiter, J. R., "The Aerodynamic Forces on Slender Plane or Cruciform Wing and Body Combinations," NACA Rept. 962, 1950.

[15]Spreiter, J. R., "On Slender Wing-Body Theory," *Journal of the Aeronautical Sciences*, 19, 1952, pp. 571-572.

[16]Heaslet, M. A. and Lomax, H., "The Calculation of Pressure on Slender Airplanes in Subsonic and Supersonic Flow," NACA TN 2900, 1953.

[17]Nielsen, J. N. and Pitts, W. C., "Wing-Body Interference at Supersonic Speeds with an Application to Combination with Rectangular Wings," NACA TN 2677, 1952.

[18]Jorgensen, L. H., "Elliptic Cone Alone and with Wings at Supersonic Speeds," NACA Rept. 1376, 1958.

[19]Mateescu, D., "Cruciform Wings and Tails Fitted with Conical Bodies in Supersonic Flow: I. Conical Flow," *Revue de Mécanique Appliquee*, Vol. 13, No. 6, 1968, pp. 1101-1121.

[20]Mateescu, D., "Cruciform Wings and Tails Fitted with Conical Bodies in Supersonic Flow: II. High Order Conical Flows," *Revue de Mécanique Appliquee*, Vol. 14, No. 1, 1969, pp. 55-76.

[21]Mateescu, D., "Aerodynamic Damping in Oscillatory Pitching Motion of Canard-Body Combinations in Unsteady Supersonic Regime," *Proceedings of Tenth Canadian Congress of Applied Mechanics*, University of Western Ontario, Canada, June 1985, pp. B75-B76.

[22]Mateescu, D., "Study of Wing Systems Fitted with Fuselages in Supersonic Regime," Ph.D. Thesis, Rom. Acad. of Sciences, June 1968.

[23]Mateescu, D. and Selescu, R., "Supersonic Flow past a Conical Body of Arbitrary Cross Section Alone or Fitted with a Delta Wing with Subsonic Leading Edges," *Studii si Cercetari de Mecanica Aplicata*, Vol. 40, Nov. 1981, pp. 819-836.

[24]Jones, D. J., "Numerical Solutions of the Flow Field for Conical Bodies in a Supersonic Stream," Canadian National Research Council, Aero. Rept. LR-507, July 1968.

[25]Mateescu, D., "Supersonic Flow Past Symmetrical Conical Bodies," IMFCA Rept. N-1468, 1975.